Patient-Specific Computational Fluid Dynamics Analysis Of Urine Flow Through Ureter

Course No.: BME-400

Submitted By-

Bashudeb Biplob Das
Student ID: 1718015

Shakib Mahmud Ayon
Student ID: 1718023

Humyra Hossain Oni
Student ID: 1718023

Submitted To-

Department of Biomedical Engineering Engineering

in partial fulfillment of the requirements for the degree of Bachelor of Science in Biomedical Engineering.

Supervised by-

Dr. Jahid Ferdous
Associate Professor
Department of Biomedical Engineering

Bangladesh University of Engineering and Technology (BUET)
Dhaka-1000, Bangladesh
17 May, 2023

Certificate of Approval

This is to certify that the thesis is the outcome of study and research done by Bashudeb Biplob Das, Humayra Hossen Oni and Shakib Mahmud Ayon under the supervision of Dr. Jahid Ferdous, Associate Professor, Department of Biomedical Engineering, Bangladesh University of Engineering and Technology (BUET), Dhaka, Bangladesh We would also like to declare the following

- This thesis has been written only to partially fulfill a requirement for the award of a graduation degree
- All contents of this document have been written by the authors, unless stated and referred.
- All external sources have been appropriately attributed

Authors

Bashudeb Biplob Das	Shakib Mahmud Ayon	Humyra Hossain Oni

Signature of the Supervisor

Dr. Jahid Ferdous

Associate Professor
Department of Biomdeical Engineering
Bangladesh University of Engineering and Technology (BUET)

Acknowledgments

We are incredibly happy to have finished our thesis on the subject of "Patient-Specific Computational Fluid Dynamics Analysis Of Urine Flow Through Ureter". First of all, we would like to express our gratitude to the Almighty for granting us perseverance, character, and—most importantly—for maintaining our health so that we could exert ourselves in finishing this text. For his helpful direction during the entire study project, Dr. Jahid Ferdous, Associate Professor in the Department of Biomedical Engineering at the Bangladesh University of Engineering and Technology, is our grateful thesis supervisor. His expertise in the field and methodical supervision helped us successfully complete our study project. He never stopped inspiring us to think creatively and to perform to the best of our abilities whenever we encountered a challenge and were stuck. His support and guidance have assisted us in enhancing our individualized skills. His priceless advice helped us with this research project get where we wanted to go. He has been a steadfast leader in our mission, and we are appreciative of that. We also hope and pray that he will carry on doing so in the near future.

We received support and encouragement from our classmates Pritom Saha and Abdullah Al Mamun while we worked on our thesis. We also want to thank our friends, our families, and everyone else who has inspired us on this path.

Abstract

Through peristaltic action, the ureter is essential in moving urine from the kidney to the bladder. However, there are a number of pathogenic factors that might impede or obstruct this movement. The goal of this work was to create ureter models with anatomical accuracy using CT scan information from six patients with normal ureters. Investigation and analysis of significant flow characteristics, such as flow velocity, pressure differential, average and maximum wall shear stresses, were the goal. We laid the groundwork for future studies into unhealthily ureteral flow by building these realistic ureter models. The study's findings serve as a standard against which to compare and assess the flow parameters of sick ureters in comparison to those of a healthy reference. This comparative analysis will be extremely helpful in determining the efficacy of therapeutic therapies and tracking the development of post-therapeutic ureteral flow. Understanding the flow parameters under study, such as flow velocity, can help one understand how quickly and unevenly urine flows down the ureter. We can better understand the forces guiding urine flow and the resistance encountered throughout the ureteral pathway by understanding the pressure difference between the inlet and output. Additionally, by analyzing the average and maximum wall shear stress, it is possible to identify potential weak points or abnormalities in the ureteral wall and learn more about the shear forces that are applied to it. These discoveries have important clinical ramifications. Healthcare providers can more accurately determine the effects of different ureteral diseases on urine flow dynamics by comparing the flow parameters of diseased ureters to those of a healthy ureter. This comparative analysis will help in the formulation of treatment plans, the making of judgments, and the tracking of the development of post-treatment ureteral function. It might also aid in the creation of individualized treatment plans that are adapted to each patient's unique needs and ureteral abnormalities. This study effectively created anatomically correct ureter models using CT scan data from six patients with healthy ureters. Investigation of the flow parameters yields vital information about the characteristics of the typical ureteral flow. Future studies analyzing abnormal ureteral flow and post-treatment assessments will build on these findings. In the end, this research advances our knowledge of ureteral diseases and moves urology closer to more efficient and individualized treatment options.

Keywords: Kidney, Ureter, Healthy Ureter, Unhealthy Ureter, 3D Model, Anatomically Correct Model, CT Scan data, Ansys, CFD Simulation, Comparison, Average Wall Shear Stress, Maximum Wall Shear Stress, Pressure Difference, Flow Velocity, Flow Parameters, Flow Simulation, Fluid Simulation, MImics, 3-Matic, Meshing, Mesh-independent Study.

Table of Contents

List of Figures

Figure **Page**

Chapter 1

Introduction

In this chapter, we provide a general overview of the ureter, what is its physiology, and which pathological reasons obstruct the ureteral flow. Furthermore, we state the motivation and consideration behind our thesis work.

1.1 Anatomy of the Ureter

The ureter, a vital component of the urinary system, can be described as a muscular tube responsible for the transport of urine from the kidneys to the bladder. With an average length ranging between 28-30 cm, shown in Figure 1.1, the ureter serves as a conduit for urine, ensuring its efficient passage through the body. The ureter's structure is characterized by thick and contractile walls, allowing it to withstand the pressure generated during the transport of urine. Its diameter varies at different points along its length, accommodating the varying flow rates and volumes of urine. This flexibility and adaptability of the ureter's diameter contribute to its efficient function in transporting urine. The movement of urine through the ureter is primarily facilitated by peristaltic muscular contractions. These contractions create a wavelike motion, propelling the urine along the length of the ureter at a uniform low speed. The coordinated contraction and relaxation of the smooth muscle fibers in the ureter walls create a sequential squeezing effect, ensuring the continuous flow of urine towards the bladder. While peristaltic contractions are the primary driving force behind urine movement in the ureter, other factors also contribute to this process. Gravity plays a role, particularly when the body is in an upright position. The force of gravity assists in the downward flow of urine, aiding the peristaltic contractions in propelling it towards the bladder. Additionally, hydrostatic pressure, resulting from the pressure exerted by the fluid within the urinary system, also assists in the movement of urine through the ureter. The ureter is equipped with a crucial mechanism known as the vesicoureteric junctions, located at the lower ends where the ureters enter the bladder. These specialized structures act as valves, ensuring the prevention of retrograde flow of urine from the bladder back into the ureter. When the bladder is filled with urine, the vesicoureteric junctions are compressed, effectively sealing

off the ureters and preventing any backward flow. This mechanism maintains the unidirectional flow of urine and safeguards the integrity of the urinary system. In conclusion, the ureter is a muscular tube that serves as a conduit for the transport of urine from the kidneys to the bladder. Its thick and contractile walls, variable diameter, and peristaltic contractions ensure the efficient movement of urine. Gravity and hydrostatic pressure contribute to urine flow, while the vesicoureteric junctions act as valves to prevent retrograde flow. Understanding the structure and function of the ureter is vital in comprehending the intricate workings of the urinary system and its role in maintaining overall health.

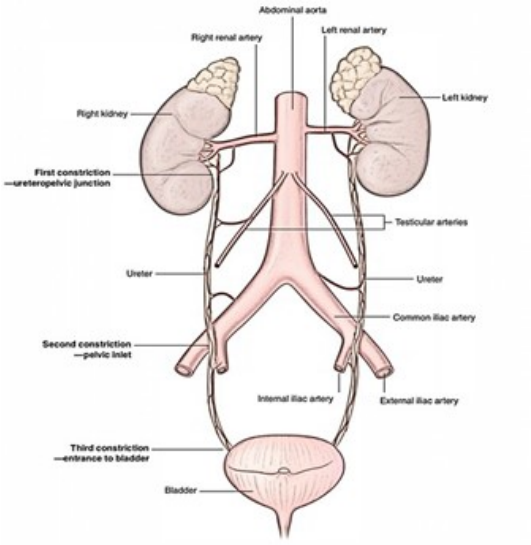

Figure 1.1: Renal system.

Both sympathetic and parasympathetic nerves innervate the ureter, which is made up of upper and lower segments. This can affect the strength and frequency of the ureter's muscles contracting. The control of urine flow through the ureters is aided by this innervation. When urine enters the renal pelvis, it creates a contraction that aids the urine's migration into the ureters. This contraction starts a chain reaction of peristaltic contractions that move the urine toward the bladder along the length of the ureter.

There are three separate layers that make up the ureter's wall, as shown in Figure 1.2, and each one has a different purpose. The mucosa is the first layer, starting from the innermost. The transitional epithelium is a specialized tissue that makes up the mucosa. This epithelium creates a continuous seal with the urinary bladder and renal pelvis lining, ensuring a strong barrier and avoiding urine leakage. The muscular coat, which is the middle layer of the ureter wall, is encountered as we move outward. This layer of smooth muscles is composed of a longitudinal layer outside and a circular layer inside. Peristalsis, or the synchronized contraction of the muscles, depends critically on the muscular coat. The wave-like motion that propels urine up the ureter and toward the bladder is created by the synchronized contraction and relaxation of the muscles through peristalsis. The adventitia is the final and outermost layer of the ureter wall. This layer, which is made of fibrous connective tissue, acts as a supporting structure. The adventitia gives the ureter structural stability by shielding it from outside influences and keeping

its shape. To enable the effective transit of urine, these three layers of the ureter wall cooperate. The muscular coat produces peristaltic contractions to force urine through the ureters while the mucosa maintains a tight seal to stop urine leaks. The ureter is supported and shielded by the adventitia. The unidirectional flow of urine is ensured by coordinated contractions, mucosal integrity, and structural support, which also contribute to a person's general health and well being.

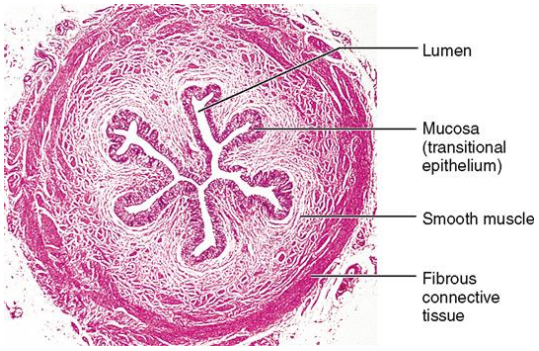

Figure 1.2: Microscopic structure of the cross-section of a human ureter.

1.2 Ureteral Physiology

The renal pelvis' pacemaker region, which is vital for the propulsion of urine into the ureter [1], is what starts the peristaltic movement. Although there is continuous discussion among academics about the precise position of the primary pacemaker, it is generally accepted that it is located in the calyceal regions closest to the renal pelvis. The major pacemaker, according to a different theory put out by Weiss et al. [2], is thought to be situated near the Pelvis Ureteric Junction (PUJ). Like the heart, the ureter also has additional muscle tissue regions known as latent pacemaker sites in addition to the primary pacemaker. In a healthy state, the major pacemakers in the renal pelvis predominate over the activity of these latent pacemakers. However, these latent pacemakers may act as pacemakers if the primary pacemakers are not prominent. The ureter has these pacemaker cells in every section. Specific pacemaker cells at the UreteroVesical Junction (UVJ) can produce antiperistalsis waves, which happen at a lower frequency than in the upper part of the ureter. Retrograde peristalsis, or the passage of urine up the ureter in the other direction, can occasionally happen. These pacemaker cells are necessary for the coordinated peristaltic passage of urine through the ureter, and their capacity to produce rhythmic contractions is one of their main functions. Understanding the function of these pacemakers and how they are distributed throughout the ureter sheds light on the intricate systems responsible for controlling urine flow.

1.3 Pathology of the Ureter

The upper tract urinary system might have the following abnormalities:

• Dysfunctional PUJ: The presence of any aberrant flow between the ureter and renal pelvis, which subsequently causes renal pelvis dilatation, is the primary indicator of dysfunctional

PUJ. A significant proportion of referrals to urologists, both adult and pediatric, are caused by dysfunctional PUJ. A example of hydronephrosis brought on by urine reflux into the renal pelvis is seen in Figure 1.3.

Figure 1.3: Conventional IntraVenous Urography image shows the hydronephrosis in left ureter in case of disfuctionality of PUJ.

• Upper Urinary Rupture: Upper ureter rupture is considered to be another serious problem. This abnormality is a perforation of the ureter and causes a series of problems such as infection and subsequent renal impairment. There are causative factors that induce ureteric rupture, including a urinary retention, extra pressure on the ureteral wall [3, 4] . Figure 1.4 shows the leakage of the left upper urinary tract due to the rupture of the proximal part of ureter.

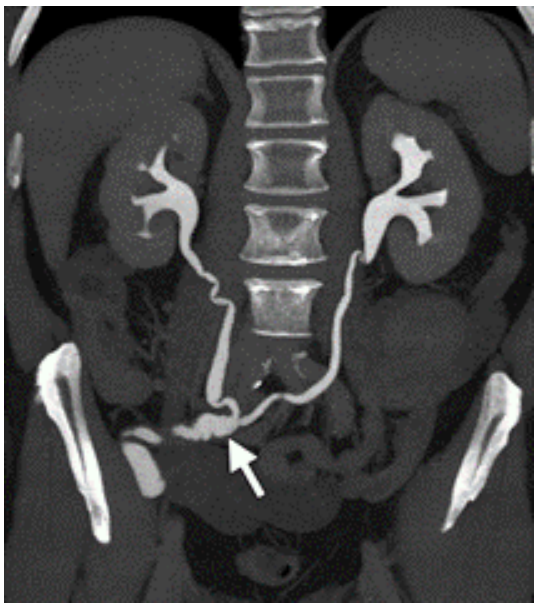

Figure 1.4: Postcontrast axial CT image shows leakage of radiocontrast media at the level of the upper ureter.

• Occlusion of the urinary pelvic junction (UPJ): Usually, a kidney stone or tumor can cause an obstruction in the urinary system, and the resulting back pressure inside the renal pelvis can be a source of further deterioration and injury.

• VesicoUreteral Reflux (VUR): This condition affects the urinary system abnormally. Due to a problem with the valves at the vesicoureteic junction, urine is backing up from the bladder into the two ureters.

• Primary megaloureter caused by obstruction: The ureter's end becomes constricted, resulting in dilatation. The constriction may be entirely functional (normal histology) or anatomical (anomaly of the muscle layer). The ureter is dilated above the constriction, and the wall is thickened. It is important to distinguish a primary megaloureter from a secondary one that is brought on by a valve or vesico-ureteral reflux. An infection of the entire urinary system may result in ureteral inflammation, which, in severe cases, causes the ureter to swell both in breadth and length.

• An abnormally high number of ureters: Partial doubling, a very uncommon disease of the ureter, is caused by the incomplete division of two ureters that re-fuse at various levels in the pelvic, lumbar, iliac, or intramural regions. According to Weigert and Meyer's law, in partial doubling of the ureters, there is a second renal pelvis and the upper ureter's orifice is located lower on the bladder than the lower ureter. This defect frequently goes undiagnosed.

• Retrocaval/Retroiliac ureter: This is an additional example of an abnormality in which the right ureter (retrocaval ureter) forms a "S" at the L4 level behind the vena cava. The pedicle of L3/4 is crossed by the right ureter's medial swing.

1.4 Peristaltic Motion

The complex action of several muscles in the ureteral wall that are misaligned results in ureteral peristaltic movements. Since it is challenging to examine a single muscle cell in isolation from its neighbors, this subject is challenging to study. According to the current view, when the circular muscles contract, the ureteral lumen narrows, and when the longitudinal muscles contract, the ureter shortens. It is important to note that along the ureter, the distribution of the longitudinal and intermediate circular muscle cells' outer and inner layers is not regular. These anatomical distributions alter the pressures acting to compress the ureteral wall, which may have an impact on how contractions spread [5]. The complicated multidimensional movements of the ureteral wall make up the ureteral peristalsis. The ureteral wall contraction affects the axial movement, axial displacement, and rotation of the ureter in addition to changes in the ureter's diameter (the transverse movement). By combining all of these movements, Osmon et al.'s analysis [6] used the video microscopic method. They demonstrated that the ureter's circumferential muscles help to enclose the urine bolus within the already-expanded ureteral segment and then help the urine bolus push into the urinary bladder by creating a vacuum effect that allows the ureter segment to fill with urine. They also discovered that a key element in boules movement is the synchronization of the longitudinal and circular smooth muscles.

1.5 Motivation

In this chapter, a realistic finite element model of the ureter system is presented. Due of the ureter's complicated and asymmetrical nature, previous research hasn't looked into its anatomically proper geometry in great detail. A high-resolution grid is necessary because of the ureter's diverse spectrum of curvatures, yet doing so increases computing time and expense. The suggested model, however, gets beyond these problems and produces computational results that closely resemble clinical data. The model enhances the quality and dependability of computational simulations and provides a more accurate representation of ureteral dynamics by adding an anatomically correct ureter geometry and enhancing the grid resolution.

Chapter 2

Literature Review

To investigate and comprehend fluid dynamics in three-dimensional (3D) ureters, many research have used computational fluid dynamics (CFD) simulations. The flow behavior, including flow rates, pressure distribution, velocity profiles, and wall shear stresses, is investigated using these models. To understand ureteral flow, researchers look at a number of variables, including ureteral shape, boundary conditions, fluid characteristics, and diseases. Realistic fluid-structure interactions and precise simulation of the intricate ureter shape are made possible by the application of cutting-edge CFD techniques and computational capacity. By refining surgical operations, creating tailored drug delivery systems, and enhancing treatment outcomes, these simulations help us better understand and treat ureteral illnesses. The knowledge gathered from these investigations has the potential to significantly improve medical interventions and advance the discipline of urology.

In this chapter, we provide short overview about the previous works done on fluid flow using CFD or FSI in a 3D ureter model.

According to Gomez-Blanco et al [7], Urologists are designing new ureteral stents to improve patient outcomes, and computational models are being used to evaluate different designs. However, due to the complexity of biological tissues, these models often have to simplify the geometry. In this study, the interaction between urine flow and a double-J stented ureter with a simplified geometry was analyzed using three different solid domain models. The study found that the interaction between the stented ureter and urine was negligible, meaning that simpler computational models, assuming the ureter is a rigid body, could be used to accurately evaluate stent designs without the need for fluid-structure interaction modeling. Despite advancements in clinical therapies for a number of ailments, there are still some limitations brought on by overly straightforward presumptions and the disregard of residual strains when thinking about the biomechanical properties of tissues.

In the study of G. Hosseini et al [8], the goal was to create a computer model that precisely depicts the ureteral system's dynamic operation, specifically its peristaltic movement under varied physiological situations. The researchers simulated the interaction between the solid ureteral

wall and the fluid flow using their proprietary coupled Cgles-Y-code fluid-solid interaction model, which included a unique immersed boundary approach. They carried out a detailed analysis of the literature on ureteral physiology with an emphasis on the peristaltic and anatomical mechanisms. Since the ureteral wall's nonlinear tensile properties were taken into account, the model's accuracy was improved over a linear one. The mesh resolution was enhanced while a geometrically realistic ureter model was built. The simulation of intra-abdominal pressure and two separate contraction models were also included in the model. The researchers looked at the urodynamic responses under various clinical circumstances, including unhealthy ureteral conditions and decreased peristalsis amplitude brought on by vasodilators. The study showed the potential of the computational model in comprehending ureteral dynamics by providing insights into shear stress distribution, urine velocity, and the potential for reflux during peristalsis propagation.

Computing models of the ureter now in use frequently lack physiological correctness in their representation of anatomical features. This paper proposes a new, more straightforward model of ureteral flow to alleviate this shortcoming. The distal portion of the ureter's peristalsis bolus is the main component of the model's simulation. The urine bolus is produced in the ureteral wall by an expanding force in a closed ureter arrangement. A computational fluid-structure interaction (FSI) simulation is used to simulate the peristaltic movement in the distal part of the ureter in order to study this phenomenon. Future research will build on these preliminary findings to create a more thorough model and examine the impact of a novel half-length ureteral stent design on urine flow. The suggested model, in the study of Vahidi et al [9], offers possible advancements in ureteral dynamics comprehension and stent design optimization for better clinical results.

In Sánchez et al [10], a novel, streamlined model of ureteral flow that focuses on replicating a peristalsis bolus in the distal region of the ureter is developed in order to overcome this constraint. In this model, an expanding force is applied to the wall of a closed ureter, which causes it to produce a urine bolus. A computational fluid-structure interaction (FSI) simulation is suggested to investigate this phenomenon by simulating the ureter's distal peristalsis movement. Although these first results offer insightful information, further effort is required to create a more comprehensive model. In order to further our understanding and maybe progress the field of ureteral interventions, it will also be examined how a novel half-length ureteral stent design affects urine flow.

In Jin et al [11], a three-dimensional urodynamic bladder-urethra system that includes the bladder, bladder neck, prostate, and urethra was created using computational fluid dynamics (CFD). The model faithfully simulates urine flow through the female urinary bladder and urethra as well as the recirculation process in the bladder during voiding. Independent of the form of the prostatic urethra, the computational results demonstrate the existence of a dead-water zone and a zone of secondary flow. An increased dead-water zone results from significant prostatic urethral constriction in cases of pathological prostate diseases. These simulation-based results can greatly improve surgical treatment for urine incontinence and serve as a basis for theoretical analysis, which will help both doctors and researchers in the field of SUI.

Niu et al [12] proposed a simpler rigid body-based lower urinary model. Simulations are run to examine the distributions of urine flow velocity, wall pressure, and shear stress along the urethra using MRI scanned uroflowmetry data from a healthy girl. As the inflow rate rises, the

numerical findings show the formation of turbulent secondary flows close to the end of the urethra. Additionally, as the flow rate reaches its maximum value, oscillations in the pressure and shear stress distributions are seen in the first part of the urethra. These discoveries help us understand the lower urinary system's flow characteristics better and shed light on the dynamics of urine flow in healthy people.

The ureter model (UM), a microfluidic device described in Carugo et al [13], is created to mimic the fluid dynamics in a stented ureter. Measurements from pig ureters served as the basis for the UM geometry. To determine the pressure in the renal pelvis compartment under various fluid viscosities, volumetric flow rates, and levels of blockage, the researchers conducted tests. These measures assisted in identifying the crucial combinations of these factors that can result in elevated kidney pressure. The study also shows how particle image velocimetry (PIV) technology might be used to examine the flow patterns inside the created microfluidic device. Overall, this research offers insightful understanding and quantification of the fluid dynamics in a stented ureter, potentially enhancing therapeutic approaches and patient outcomes.

The therapeutic potential of integrating CFD with existing techniques in human tract analysis, secondary flow effects, disease prevention, and non-invasive diagnostics is suggested by the accuracy of the models in Singla et al [14].

For a combination of the three different ureters, with and without a ureteral stenosis, and with four different types of double J stents, a numerical analysis of the urine flow rate and pattern in the ureter was carried out by Kim et al [15]. The urine flow rate and pattern varied between the three ureters. Shape of the ureter has an impact on luminal flow rate. Depending on the geometry of the ureter, the side holes of a double J stent had a variable role in diversion.

In Razavi et al [16], numerical simulations were used to examine the flow of urine during peristalsis in the ureter with vesicoureteral reflux (VUR) and posterior urethral valves (POM). Fluid-structure interaction (FSI) was used to describe peristalsis and capture interactions between urine and elastic walls. The simulations made use of the Newtonian fluid behavior, incompressible Navier-Stokes equations, and wall elasticity theories. With VUR and POM, velocity fields, viscosity stresses, and volumetric outflow rates were calculated for the ureter during peristalsis. Additionally, the effect of urine viscosity on flow rate was investigated. The findings demonstrated that elevated bladder pressure caused VUR as a result of malfunction at the ureterovesicular junction, which placed high strains on the wall. In the instance of POM, the outflow rate fell to nil and there were significant strains in the part that was blocked. Comparing the findings showed that at high bladder pressures, reflux occurred in the ureter with VUR, and peristalsis further enlarged the prestenotic region. Additionally, peristaltic ureters had higher urine velocities than non-peristaltic ureters.

In Najafi et al [17], the study looked at the peristaltic movement of the ureter both with and without stones using three-dimensional computational fluid dynamics (CFD) simulations using the program ANSYS Fluent. Through a number of simulations, the impacts of stone size and form were investigated. Three stone forms (sphere, cube, and star) were tested at a fixed blockage percentage of 15% whereas fixed spherical stones were examined at different obstruction percentages (5%, 15%, and 35%). To comprehend the effects of these variables, velocity vectors, mass flow rates, pressure gradients, and wall shear stresses were examined. The findings demonstrated that as

obstruction increased, there was an increase in backflow, pressure gradients, and wall shear stresses close to the stone. The biggest backflow was produced by cube-shaped stones, whereas the highest-pressure gradient magnitudes were produced by star-shaped stones. Notably, at the measured blockage level, the change in stone shape had no discernible impact on the wall shear stress.

A mathematical model is created in Siggers et al [18] to evaluate urine flow in a stented ureter. The ureter wall is viewed as a non-linear elastic membrane in the model, which also assumes axisymmetry. A hard, permeable, hollow, circular cylinder implanted inside the ureter is how the stent is visualized. When the internal pressure rises, the renal pelvis expands like an elastic sack. From the kidney, fluid enters the renal pelvis at a specific rate. Urine fills the stent, ureter, and renal pelvis, and the bladder's pressure is managed. The model is used to determine how the characteristics of the stent and ureter affect the overall amount of reflux produced as the bladder's pressure rises.

Chapter 3

Methodology

3.1 Development of a Finite Element Model for the Ureter

Six CT scans in total, from various hospitals, were gathered to acquire data for the study. Patients over the age of 30 who were both male and female underwent these scans. Each image was carefully examined to make sure there were no obstructive elements or disconnections. The 350 DICOM pictures, each with a thickness of 1.5 mm, were used to construct the CT scans. The analysis and simulation of the urinary systems in the research study are made possible thanks to this extensive dataset.

3.2 Model generation

The image-processing tool Mimics 21.0, created by Materialise Company, was used to import and process the CT scans. This software was created specifically for the processing of medical images, and it allows the integration of several 3D medical image segmentations obtained from CBCT, micro-CT, CT, and MRI scans as well as 3D ultrasound and confocal microscopy. Mimics enables the production of precise and accurate 3D models that accurately depict a patient's anatomical structures by utilizing these imaging data sources. This robust program offers a complete method for importing, segmenting, and building 3D models from medical photos, allowing researchers to precisely see and examine the important anatomical aspects.

With an in-plane resolution of 0.80 mm and a slice to slice spacing of 1.5 mm, a data set of more than 6 transverse CT scan slices was processed for this study. Unaltered scans of the coronal, transverse, and sagittal planes in Mimics are shown in Figure 3.1, 3.2, and 3.3.

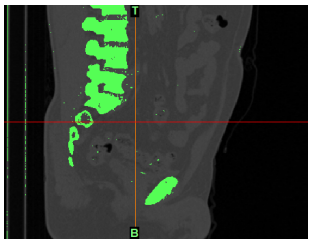

Figure 3.1: (Coronal Plane

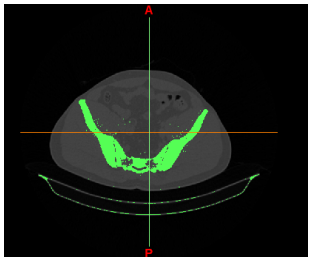

Figure 3.2: (Transverse Plane

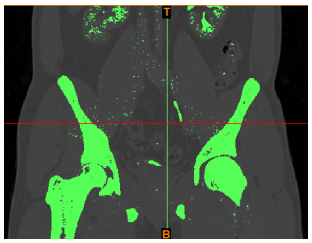

Figure 3.3: Sagittal Plane

The surrounding soft tissue should be removed from the CT images of the ureter. The thresholding function in Mimics, which recognizes the greyscale regions in the photos with values between 260 and 3071, was used to do this. The average length and diameter of the ureter are approximately 239.95 mm and 5.06 mm, respectively, as shown in Figure 3.4, which is an extracted 3D model of the ureter from the original scanned images.

Figure 3.4: (Unmodified 3D ureter model)

Parts of the bladder and renal pelvis are represented by the yellow areas at the bottom and top of the figure. The bladder and renal pelvis were disregarded and eliminated from the model to leave only the ureter because we are only interested in the computational study of the ureter.

By manually removing the bladder and renal pelvis portions, this was accomplished. The ureter, which measures 199.52 mm in length, is depicted as a cropped 3D model in Figure 3.4. It is evident that there are deformations, which we interpret as being caused by peristaltic contractions. The created 3D model can be used to determine the diameter and length of the ureter, however due to its microscopic scale and repeated cross-sectional changes throughout its length, this model was unable to provide a precise geometrical description. Utilizing the Mimic software, the center line of the 3D geometry was found, and the resulting 3D model provided a reasonable approximation of the ureter geometry. The intricate geometry of the iliac arteries is maintained in this model. This model is more intricate than the one that was utilized in earlier computer research [19], in which the ureter's form was reduced to a thick-walled tube.

3.3 Flow Simulation

The generated 3D model is then imported for fluid flow simulation. For our study, we have used ANSYS 2022R1 to run CFD simulation for analyzing flow parameters (flow velocity, pressure difference, average wall shear stress and maximum wall shear stress). The computational modeling and study of fluid flow, heat transfer, and other related processes is known as CFD simulation, and it is carried out using software such as ANSYS. The Navier-Stokes equations and other governing equations for fluid dynamics are solved using numerical techniques. The computational domain is represented by a discretized mesh in ANSYS CFD simulations, which simulates fluid behavior and interactions with solid barriers. ANSYS CFD models help in the design and optimization of diverse engineering systems and processes by offering insightful information about complex fluid flow patterns, temperature distributions, pressure gradients, and other crucial factors through iterative computations.

3.4 Meshing of Ureter model

An essential part of computational fluid dynamics (CFD) simulations carried out with ANSYS software is mesh analysis. To enable the numerical solution of the governing equations for fluid flow and related phenomena, the computational domain in CFD is discretized into a mesh or grid of smaller pieces.

The meshing procedure in ANSYS entails segmenting the domain into a group of connected cells or elements. Depending on the particular needs of the simulation, a different form of mesh may be employed. Structured meshes, unstructured meshes, and hybrid meshes are typical mesh types. Regularly formed pieces, like quadrilaterals or hexahedra, make up structured meshes. For simpler geometries, these meshes provide advantages in terms of accuracy and computational effectiveness. On the other hand, irregularly shaped pieces like triangles or tetrahedra are used in unstructured meshes. They have greater flexibility and work well with complicated geometries with erratic bounds. In order to balance accuracy and computing economy, hybrid meshes blend organized and unstructured features.

The accuracy and convergence of the CFD simulation are highly dependent on the mesh quality. The numerical solution will accurately resolve gradients and capture key flow features if the mesh is well-structured and polished. Higher densities exist where flow gradients or complicated

processes take place, with mesh densities, or the number of cells, varying over the domain. In order to perform an effective mesh analysis in ANSYS, one must first assess the mesh quality, look for problems like distorted or skewed elements, and then optimize the mesh to reach the necessary computational accuracy and efficiency. To increase mesh quality and solution convergence, iterative refinement and mesh adaption techniques can be used. We have thoroughly tested the mesh independence of all the used models in order to guarantee the accuracy and reliability of our study. The goal of this test is to identify the ideal mesh refinement level that yields accurate results with minimal computing overhead. The developed models had about 2.4 million elements total in our analysis. These are all tetrahedral elements, which are frequently used in CFD simulations. Tetrahedral elements may effectively represent complex geometries with erratic borders due to their versatility.

We systematically assessed the effect of mesh density on the outcomes by altering the number of pieces in the mesh. Starting with a rough mesh, we gradually fine-tuned it until the solution no longer changed significantly with mesh refinement. We were able to identify the point of mesh independence through this procedure, which is the point at which further mesh refining does not result in appreciable improvements to the solution.

In our analysis, it was determined that the element count of roughly 2.4 million was an appropriate choice for obtaining precise and trustworthy results. This mesh size balances the need for less computing resources while yet capturing key flow aspects. Tetrahedral elements provide advantages in effectively capturing flow characteristics and modeling complicated geometries in our mesh. Tetrahedral meshes ensure accurate resolution of flow gradients and boundary layers by adapting to regions of interest and conforming well to uneven boundaries.

The visual representation of the mesh in Figure 3.5 draws attention to how the tetrahedral pieces are distributed throughout the computational area. With the use of this representation, we can see how the domain has been discretized and the degree of refinement attained.

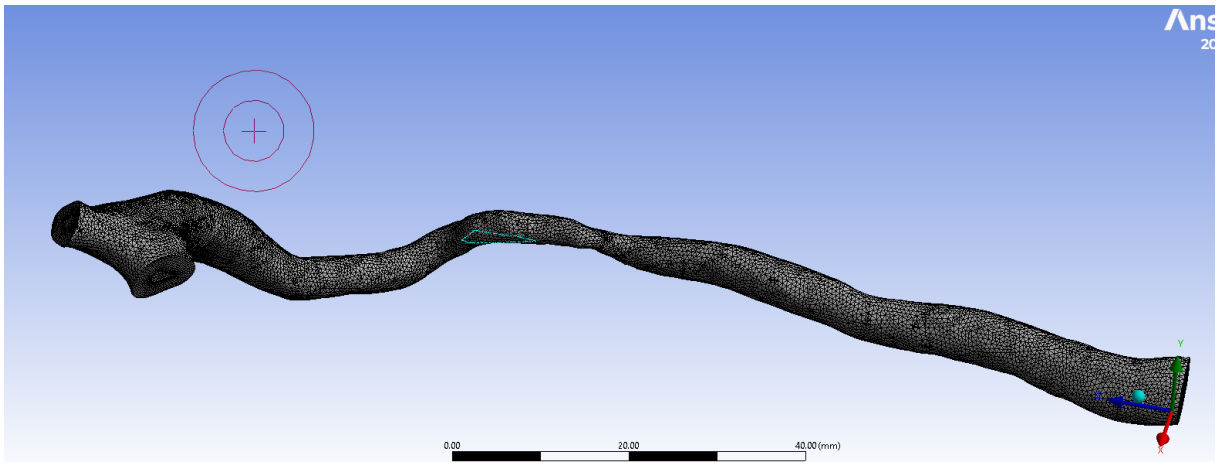

Figure 3.5: (Mesh analysis)

3.5 Boundary Conditions

We take into account a fluid with a density (ρ) of $1050 kg/m^3$ and a viscosity (μ) of $1.3cP$ (centipoise) in our fluid flow study. These characteristics play a key role in describing how the

fluid behaves during the simulation.
We set a "no slip" boundary constraint to guarantee correctness in our simulation. This presumption asserts that the fluid conforms to the domain's borders, which means that the fluid's velocity at the boundary is equal to the solid surface's velocity. Numerous real-world situations, such as when a liquid pours over a solid object, fit this requirement.
A velocity inlet and a pressure outlet boundary condition define the fluid flow. We provide a normal entrance velocity of $2cm/s$ (centimeters per second) at the velocity inlet. This determines the fluid's entry velocity, which affects the general flow behavior. We are able to regulate and modify the flow characteristics at the intake boundary thanks to the velocity inlet condition.
We established an optimum outlet pressure of $0.3Pa$ (Pascal) at the pressure outlet border. The pressure of the fluid when it leaves the domain is determined by this circumstance. A pressure gradient is created within the domain by setting the outlet pressure, which affects the flow behavior and offers a realistic depiction of fluid dynamics.
These boundary conditions allow us to create a clear flow situation for our simulation. Within the computational domain, the density and viscosity of the fluid as well as the boundary conditions are key factors in establishing the flow characteristics, pressure distribution, and velocity profile. We can learn a lot about the behavior of the fluid system under study by precisely describing these features.

3.6 Governing equation

The fluid under investigation, urine, is described as a homogenous substance with consistent qualities throughout its composition. It is regarded as a viscous fluid, which means that it resists flow, and it is incompressible, retaining a constant density despite changes in pressure. Based on these presumptions and Newton's rule of viscosity, urine is categorized as a Newtonian fluid.
The governing equations of fluid dynamics were used to mathematically model and simulate the behavior of urine flow in the ureter. These equations include the Navier-Stokes equation and the continuity equation, which both express the conservation of mass and momentum, respectively. These formulas are essential for comprehending and forecasting fluid dynamics.
The discretization method was used in the study to convert these controlling equations into a set of algebraic equations. For this, the finite volume approach was specially used. By separating the computational domain into discrete control volumes, this numerical technique enables the approximation and solution of the equations inside each volume. The accuracy and versatility of the finite volume method make it a popular choice for CFD simulations. The continuity and momentum equations are shown below:

$$\nabla \cdot \mathbf{u} = 0 \tag{3.1}$$

$$\frac{\partial \mathbf{u}}{\partial t} + (\mathbf{u} \cdot \nabla)\mathbf{u} = -\frac{1}{\rho}\nabla p + \nu \nabla^2 \mathbf{u} + \mathbf{f} \tag{3.2}$$

where $\mathbf{u}$ is the velocity vector, t is time, ρ is the fluid density, p is the pressure, ν is the kinematic viscosity, ∇ is the gradient operator, and $\mathbf{f}$ represents any external body forces acting on the fluid.. The Semi-Implicit Method for Pressure-Linked Equations (SIMPLE) algorithm deals with

the pressure terms in the momentum equations and uses the iterative procedure in which the solution to the discretized equations is obtained.

Chapter 4

Results and Discussions

4.1 Mesh-independent study

By changing the amount of mesh elements, the study's geometry parameter was examined. It was found that the parameter value converged to a saturation point when the number of elements rose and the mesh size shrank. In particular, it was discovered that the average wall shear stress was 0.7301 Pa when the element number was 11,04,109. After that, the mesh size was reduced, producing 24,39,630 elements—almost twice as many as before—with an average wall shear stress of 0.729 Pa. Between the two examples, there was hardly any change in the average wall shear stress, as shown in Figure 4.1. Based on these results, a body size of 0.5 mm and a coordinate size of 0.45 mm were selected for the simulation.

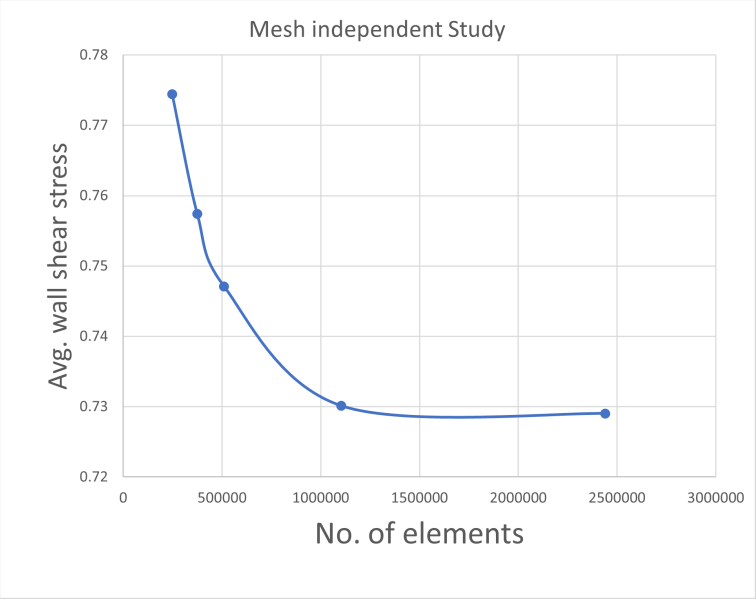

Figure 4.1: (Mesh independent study)

4.2 Flow Parameters

In this study, we carried out a thorough investigation of numerous flow characteristics derived from CFD simulations of six distinct ureter models. We concentrated on analyzing the average and maximum wall shear stresses, flow velocity, pressure differential, and wall shear stress in these models.
We calculated the velocity profiles across the flow domain by modeling the fluid dynamics within each ureter model. This gave information about how the flow velocity changed along the ureter's length and in other regions of interest. In order to better understand the pressure distribution within the urinary system, we also looked into the pressure difference between the input and outflow ends of the ureter.
We focused particularly on the ureter walls' exposure to wall shear stress. At various sites, we calculated the maximum wall shear stress as well as the average wall shear stress. These variables gave important information regarding the stresses that the urine flow exerted on the ureter walls. It is crucial to comprehend wall shear stress in order to evaluate the likelihood of urinary system damage or difficulties.

4.2.1 Pressure Contour

We included velocity inlet and pressure outlet boundary conditions in our simulation. This means that while the pressure at the input may change based on the circumstances, the pressure at the output is fixed. We see that the pressure progressively drops as we descend from the intake.
The pressure is rather high at the inlet, where the fluid enters the system. This is due to an increase in pressure at the site of entrance caused by the fluid being actively supplied or forced into the system. Following the flow channel, we move downward through the system and experience a drop in pressure, as shown in Figure 4.2.

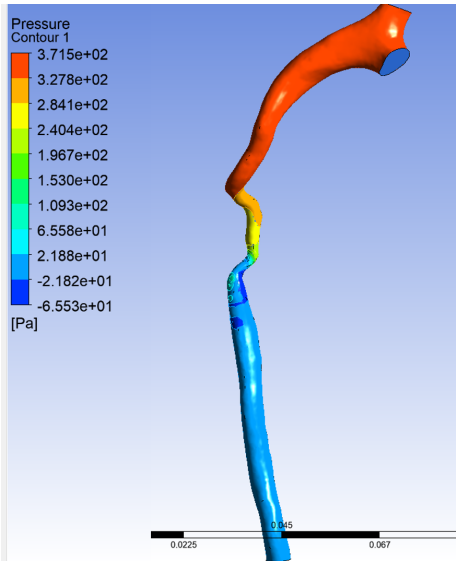

Figure 4.2: (Pressure Contour)

There are a number of reasons for the pressure drop along the flow path. These include the resistance the fluid faces as a result of geometrical changes, frictional losses, or energy loss inside

the system. The fluid experiences changes in velocity as it passes through the geometry and comes into contact with various areas that could have an impact on the pressure distribution.

4.2.2 Wall Shear Contour

The wall shear contour offers important information on how the wall shear stress is distributed across the geometric body. The frictional force applied by the fluid to the geometry's surface is referred to as wall shear stress. We can see how the degree of shear stress varies across the body by examining the wall shear contour.

We note that the wall shear contour in our simulation displays different color variations along the geometry. These differences in hue represent variations in the strength of the wall shear stress. The body has a minor bend or curve in the center, which correlates to a location where wall shear stress is produced at a higher rate than in other areas of the geometry, as shown in the Figure 4.3.

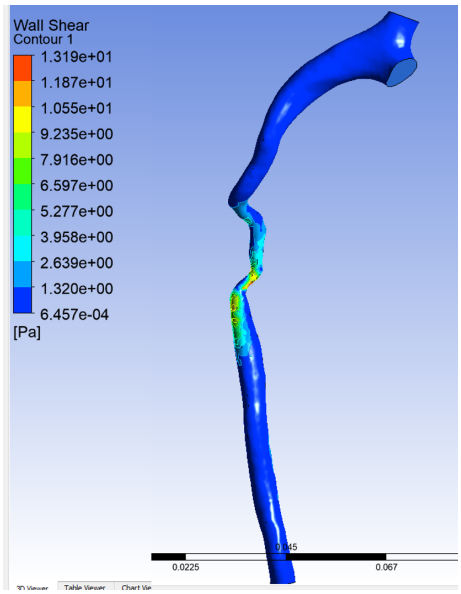

Figure 4.3: (Wall Shear Stress Contour)

The unique properties of the geometry and the fluid flow dynamics can be used to explain this rise in wall shear stress at the center of the body. There is a higher velocity gradient experienced by the fluid molecules in this area, increasing the frictional forces acting on the body's surface. As a result, this segment has more wall shear stress than other sections.

4.2.3 Velocity Streamline

We also looked at the velocity contour, which shows the velocity profile across the targeted geometry. We found that the boundary conditions, especially near the intake, have an impact on the velocity distribution. The upper section of the body displayed higher velocities than the bottom part since we defined a velocity inlet as the boundary condition, as shown in Figure 4.4.

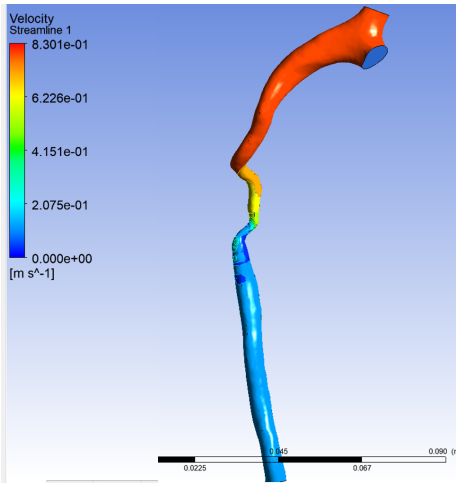

Figure 4.4: (Velocity Streamline)

4.3 Comparison of Patient Data

Inlet and output pressure differences are referred to as pressure difference. The outlet flow pressure was set for steady flow at 0.3 Pa, however the inlet pressure fluctuates continually with inlet velocity. High inlet pressure was accompanied by high inlet velocity, as shown in Figure 4.5.

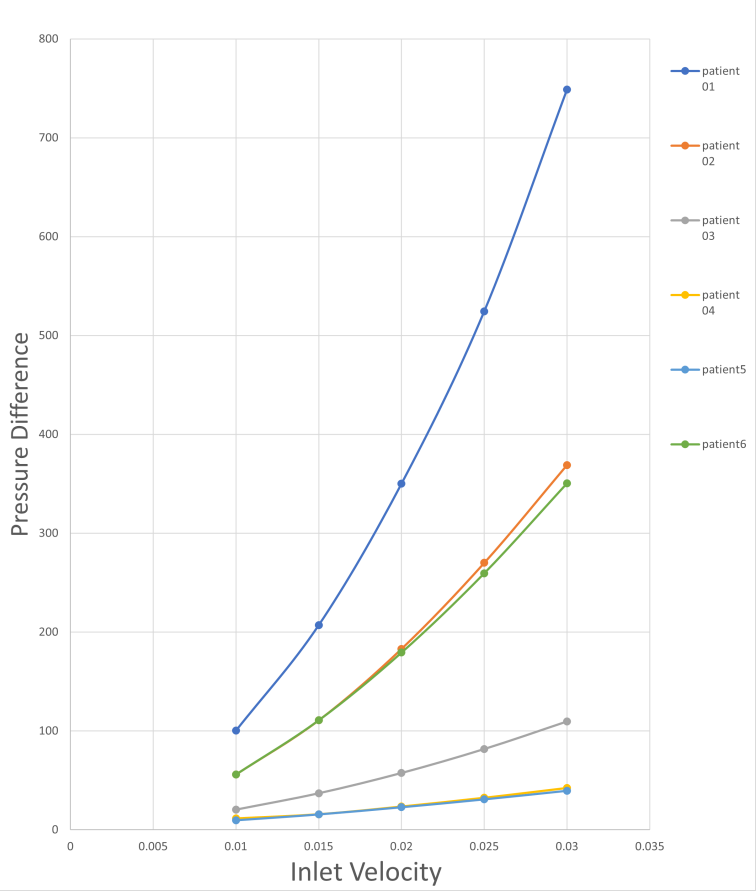

Figure 4.5: (Pressure Difference for different patients)

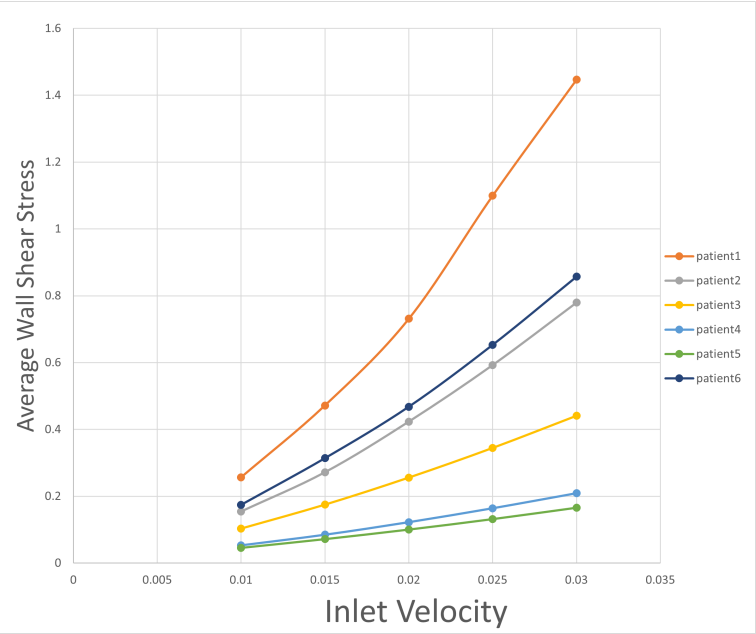

Figure 4.6: (Average wall shear stress for different patients)

Figure 4.6 shows the average wall shear stress as a function of input velocity. The plot indicates that the average wall shear stress may vary from patient to patient, but there is no doubt that the average WSS rises as velocity increases.

Plots of maximum wall shear stress that are patient-specific belong to inlet velocity. The max WSS also rises with rising input velocity; six patients' outputs demonstrate this trend, shown in Figure 4.7. The maximum WSS for patient 1 is 17.919 Pa at an inlet velocity of 0.03 m/s, whereas for patient 4 it is 0.03 Pa. 17.88 Pa is the greatest wall shear difference.

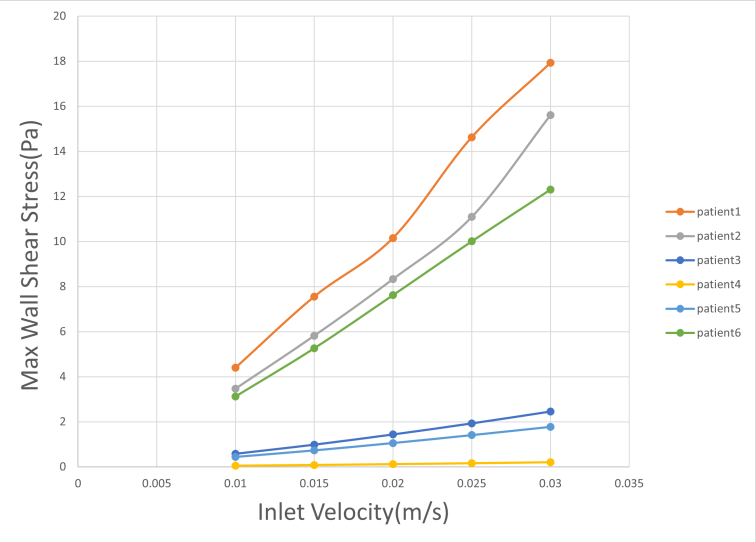

Figure 4.7: (Maximum wall shear stress for different patients)

For all patients, the outlet velocity patterns found in our study consistently demonstrate a close association with the inlet velocity. This suggests that as inlet velocity rises, outflow velocity must follow suit, shown in Figure 4.8.

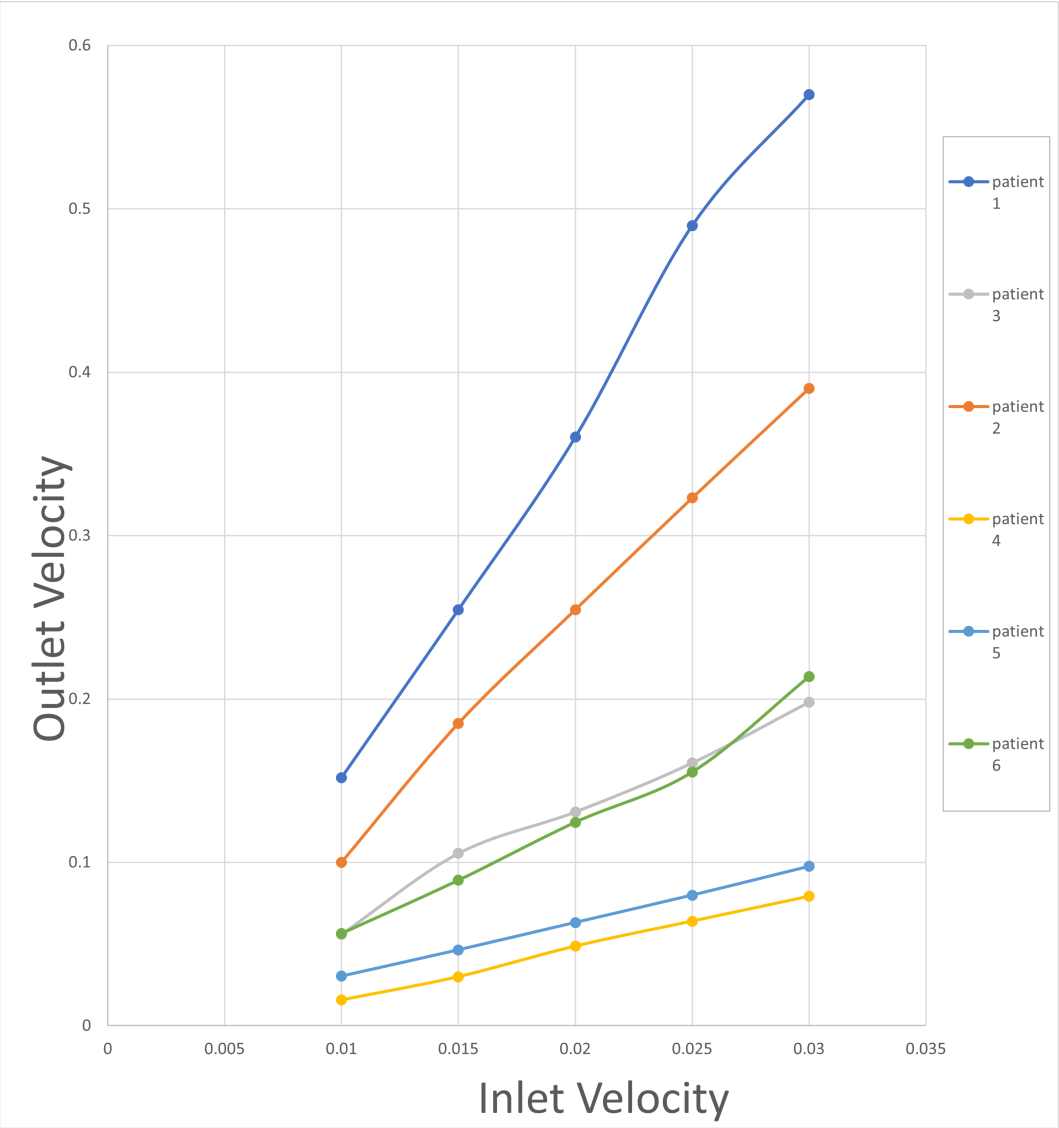

Figure 4.8: (Output velocity for different patients)

4.4 Discussion

The conservation of mass principle and the system's flow characteristics are to blame for this connection. The fluid has greater momentum and kinetic energy when it enters the system at a higher intake velocity. This momentum is redistributed as the fluid moves through the system as a result of different interactions, including fluid-fluid and fluid-geometry interactions.

The average wall shear stresses at various velocities in our investigation are shown in Figure 4.9. It demonstrates a continuous relationship between rising velocity and rising average wall shear stress. It can be assumed that an unhealthy ureter, such as one impacted by stenosis, ureter stone, or ureter constriction, would exhibit higher average wall shear stresses outside the range shown in this chart since we have concentrated on healthy patient data in this analysis.

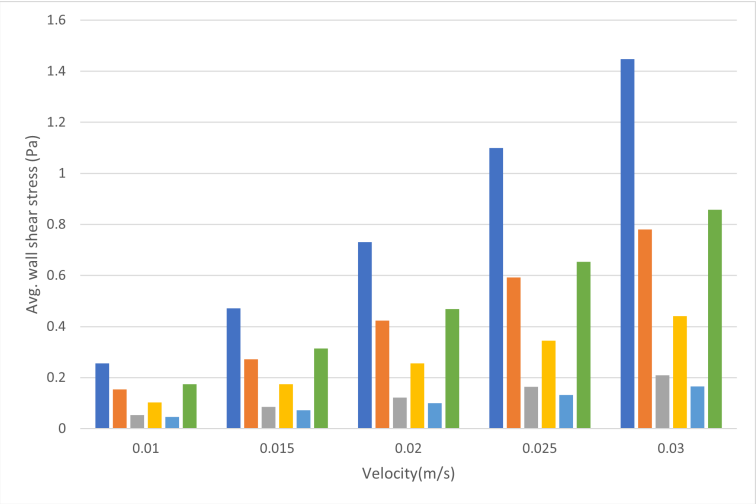

Figure 4.9: (Different avg. wall shear stress in different velocity)

Prior to surgery, the ureter-related parameters in a patient with a ureteral disease are anticipated to be higher relative to the normal range. However, these values should go below the level of normal after the surgical intervention, and this can be measured by simulation.
The bar chart serves as a starting point for comparing the typical wall shear stress of a healthy ureter with that of an unwell ureter. While it is impossible to predict exact values for any given ailment, the table can be used to assess how different situations affect various ureteral metrics. This facilitates preoperative and postoperative evaluations, enabling quantitative evaluation of surgical intervention effectiveness and restoration of ureteral parameters to normal or close to normal values.

Chapter 5

Limitations

Our investigation ran into a number of obstacles and restrictions that compromised the precision and dependability of our findings. These issues were caused by a lack of data, noisy CT scan data, an ambiguous depiction of the ureter in the CT scans, unworkable simulation models, trouble determining the right boundary conditions, and a dearth of recent research in patient-specific ureter flow simulation.

The lack of readily available data was one of our biggest problems. Accurate representation of the anatomical and physiological features of the ureter was hampered by the limited availability of patient-specific data and pertinent studies. The quality and realism of our simulations were greatly hampered by this data shortage.

In addition, the CT scan data we did receive was noisy, comprising aberrations and distortions that harmed the ureter's representation's clarity and accuracy. Our models and subsequent simulations have uncertainties and probable inaccuracies due to these noise-related problems.

Additionally, the visibility of the ureter was frequently hazy in the images from the CT scans. It was difficult to adequately represent the geometry and size of the ureter in our models because of the absence of distinct boundaries and finely detailed components. The accuracy of our models and the subsequent examination of urine flow within the ureter were both impacted by this uncertainty.

The simulations' unworkable models further complicated the investigation. The credibility of the results from the simulations was hampered by the difficulty to faithfully reflect the anatomical characteristics of the ureter due to data and image quality restrictions. Under realistic conditions, it became challenging to fully represent the complex fluid dynamics occurring within the ureter.

Additionally, finding appropriate boundary conditions turned out to be a big difficulty because there isn't much recent research on patient-specific ureter flow simulation. The selection of proper boundary conditions was difficult because there were no recognized standards or references, which resulted in uncertainties in the simulation setup.

Last but not least, our capacity to test and evaluate the correctness of our findings was constrained

by the lack of appropriate reference or benchmark data to compare against the results generated from our simulations. Our ability to accurately assess the performance and integrity of our simulation models was hampered by the absence of a trustworthy reference.

Despite these obstacles and constraints, we worked hard to lessen their effects and carried out our research as skillfully as we could while recognizing the inherent uncertainties. To increase the accuracy and dependability of patient-specific ureter flow simulations in next research projects, it is critical to overcome these limitations and keep working to improve data collecting, imaging quality, and modeling methodologies.

Chapter 6

Future Works

The collection of a larger and more varied dataset of patient-specific data will be a key emphasis in upcoming work to assure an accurate comparison between healthy and sick ureters. We can increase the robustness and generalizability of our findings by incorporating a wider range of patient data, including people with diverse ages, genders, and medical problems.
To do this, efforts might be made to coordinate with numerous healthcare organizations and form alliances in order to gather a greater pool of patient data. We have access to a larger variety of CT scan data, medical records, and diagnostic data by collaborating closely with healthcare professionals and researchers. This would allow us to create a thorough database of the ureter properties unique to each patient, including both healthy and pathological states.
We can learn more about the effects of different factors on ureter function by contrasting the ureter flow patterns and dynamics in healthy people and those with particular diseases or pathologies. This would help us comprehend how conditions affecting the urinary system, such as kidney stones, ureteral strictures, or infections, alter the behavior of the flow within the ureter.
Additionally, with a larger dataset, statistical analysis could be done and stronger relationships between ureter shape, patient demographics, and flow parameters might be found. As a result, individualized treatment strategies could be developed using prediction models that can calculate ureter flow patterns based on unique patient features.
Future research should concentrate on standardizing imaging methods, guaranteeing uniform picture quality and resolution across various medical facilities, in order to assure accurate and reliable comparisons. As a result, the obtained CT scan data would be less variable and the ureter depiction would be more accurate and clearer.
Additionally, using computational methods, such as machine learning algorithms, can help with automated CT scan data segmentation and analysis, facilitating the effective extraction of pertinent information and boosting the accuracy of the results.
Future research could provide a more thorough understanding of ureter flow dynamics in both healthy and diseased settings by enlarging the patient data set and adding cutting-edge computational approaches. For illnesses of the urinary system, this increased dataset and cutting-edge

computer analysis can help with better treatment planning, precise diagnosis, and the creation of patient-specific medicines. By utilizing these developments, researchers can further their understanding of the intricate dynamics of ureter flow, resulting in more efficient and customized therapies that increase patient outcomes and the overall health of the urinary system.

Chapter 7

Conclusion

By using CT scan data from six patients to create a model of the ureter, our study aims to examine the flow parameters of a healthy ureter. To examine flow properties such flow velocity, pressure differential, average wall shear stress, and maximum wall shear stress, computational fluid dynamics (CFD) simulations were run. The data acquired serve as a foundation for comparisons with sick ureters in the future and offer useful insights into the flow behavior of a healthy ureter.

We have prepared the groundwork for evaluating the effectiveness of therapeutic interventions in patients with ureteral problems by determining the flow parameters for a healthy ureter. We may simulate post-treatment ureter flow using the simulation-based method and compare the flow characteristics to those of a healthy ureter. This comparison analysis will help in assessing the development and efficacy of treatment in ureteral function restoration.

Important information about the flow properties of a healthy ureter was discovered by the CFD simulations. The flow velocity profiles revealed a recurrent pattern, with the upper portion of the ureter exhibiting higher velocities than the lower portion. According to the pressure difference study, the ureter's entrance pressure was higher than its outflow pressure and gradually decreased over its entire length. The distribution of shear pressures along the ureter wall was also shown by the examination of average and maximum wall shear stress, with larger values seen at specific areas such bends or curves.

These results open the door for more research into the flow characteristics of diseased ureters. We can better comprehend the effects of various ureteral diseases, such as stenosis, stones, or constriction, on the flow parameters by contrasting the flow characteristics of sick ureters with those of a healthy reference. We will be able to monitor the effectiveness of therapeutic therapies and evaluate the success of ureteral flow restoration thanks to this comparison analysis.

In summary, using patient CT scan data and CFD simulations, this study was able to calculate

the flow characteristics for a healthy ureter. The obtained data serve as a starting point for comparisons with ureters in good condition in the future, making it easier to gauge treatment success and return of regular ureteral flow. The results show potential for improving patient outcomes in the field of urology and progress the development of individualized therapeutic approaches for ureteral disorders.

Bibliography

[1] Christos E. Constantinou. Renal pelvic pacemaker control of ureteral peristaltic rate. *The American journal of physiology*, 226 6:1413–9, 1974.

[2] WEISS R. M. Localization of pacemaker for peristalsis in the intact canine ureter. *Invest. Urol.*, 5:42–48, 1967.

[3] Seung-Kwon Choi, Solmin Lee, Sunchan Kim, Tae Gu Kim, Koo Han Yoo, Gyeong Eun Min, and Hyung-Lae Lee. A rare case of upper ureter rupture: Ureteral perforation caused by urinary retention. *Korean Journal of Urology*, 53:131 – 133, 2012.

[4] E. Pampana, Simone Altobelli, Marco Morini, Aurora Ricci, Silvia D'Onofrio, and Giovanni Simonetti. Spontaneous ureteral rupture diagnosis and treatment. *Case Reports in Radiology*, 2013, 2013.

[5] Alan J. Wein, Louis R. Kavoussi, Andrew C. Novick, Alan W. Partin, and Craig A. Peters. Comprar campbell-walsh urology 10th edition review, 10th edition | alan j. wein | 9781437723939 | saunders. 2011.

[6] Fares Osman, György L Nádasy, Emil Monos, Péter Nyirády, and Imre Romics. A novel videomicroscopic technique for studying rat ureteral peristalsis in vivo. *World Journal of Urology*, 27:265–270, 2009.

[7] J. Carlos Gómez-Blanco, F. Javier Martínez-Reina, Domingo Cruz, José B. Pagador, Francisco Miguel Sánchez-Margallo, and Federico Soria. Fluid structural analysis of urine flow in a stented ureter. *Computational and Mathematical Methods in Medicine*, 2016, 2016.

[8] Ghazaleh Hosseini. Computational simulation of urinary system. 2017.

[9] Bahman Vahidi and Nasser Fatouraee. A biomechanical simulation of ureteral flow during peristalsis using intraluminal morphometric data. *Journal of Theoretical Biology*, 298:42–50, 2012.

[10] Enrique Mancha Sánchez, Juan Carlos Gómez Blanco, Julia Estíbaliz de la Cruz Conty, Francisco Manuel Sánchez Margallo, José B. Pagador Carrasco, and Federico Soria Gálvez. Simplified model of ureteral peristalsis bolus using fluid structure interaction. 2020.

[11] Qinghua Jin, Xiaojun Zhang, Xiaoyan Li, and Jianliu Wang. Dynamics analysis of bladder-urethra system based on cfd. *Frontiers of Mechanical Engineering in China*, 5:336–340, 2010.

[12] Yang-Yao Niu and Dingyong Chang. Cfd simulation of shear stress and secondary flows in urethra. *Biomedical Engineering: Applications, Basis and Communications*, 19:117–127, 2007.

[13] Dario Carugo, M. ElMahdy, X. Zhao, Marcus J. Drake, Xunli Zhang, and Francesco Clavica. An artificial model for studying fluid dynamics in the obstructed and stented ureter. *2013 35th Annual International Conference of the IEEE Engineering in Medicine and Biology Society (EMBC)*, pages 5335–5338, 2013.

[14] Nirmish Singla, Ajay Kumar Singla, and Joon Sang Lee. A novel, non-invasive approach to diagnosing urinary tract obstruction using cfd. *Journal of young investigators*, 18 6, 2008.

[15] Hyoung-Ho Kim, Young Ho Choi, Seung Bae Lee, Yasutaka Baba, Kyungwuk Kim, and Sang-Ho Suh. Numerical analysis of the urine flow in a stented ureter with no peristalsis. *Bio-medical materials and engineering*, 26 Suppl 1:S215–23, 2015.

[16] Seyed Esmail Razavi and Mohammad Jouybar. Fluid-structure interaction simulation of ureter with vesicoureteral reflux and primary obstructed megaureter. *Bio-medical materials and engineering*, 29 6:821–837, 2018.

[17] Zahra Najafi, Prashant Kumar Gautam, Bradley F. Schwartz, Abhilash J. Chandy, and Ajay Mahajan. Three-dimensional numerical simulations of peristaltic contractions in obstructed ureter flows. *Journal of biomechanical engineering*, 138 10, 2016.

[18] Jennifer H. Siggers, Sarah L. Waters, Jonathan A. D. Wattis, and Linda J. Cummings. Flow dynamics in a stented ureter. *Mathematical medicine and biology : a journal of the IMA*, 26 1:1–24, 2008.

[19] Bahman Vahidi and Nasser Fatouraee. A numerical simulation of peristaltic motion in the ureter using fluid structure interactions. *2007 29th Annual International Conference of the IEEE Engineering in Medicine and Biology Society*, pages 1168–1171, 2007.